Light-Driven Transformation Processes of Anisotropic Silver Nanoparticles

George P. Lee,[†] Yichao Shi,[†] Ellen Lavoie,[‡] Torben Daeneke,[†,⊥] Philipp Reineck,[†] Ute B. Cappel,[†,¶] David M. Huang,[§] and Udo Bach[†,⊥,∥,*]

[†]Department of Materials Engineering, Faculty of Engineering, Monash University, Clayton 3800, Victoria, Australia, [‡]Monash Centre for Electron Microscopy, Building 81, Wellington Road, Clayton 3800, Victoria, Australia, [§]School of Chemistry & Physics, The University of Adelaide, SA 5005, Australia, [⊥]Commonwealth Scientific and Industrial Research Organization, Materials Science and Engineering, Clayton South, Victoria 3169, Australia, and [∥]Tech Fellow, The Melbourne Centre for Nanofabrication, 151 Wellington Road, Clayton 3168, Victoria, Australia. [¶]Present address: Department of Chemistry, Imperial College London, South Kensington Campus, Exhibition Road, London SW7 2AZ, U.K.

ABSTRACT The photoinduced formation of silver nanoprisms from smaller silver seed particles in the presence of citrate anions is a classic example of a photomorphic reaction. In this case, light is used as a convenient tool to dynamically manipulate the shape of metal nanoparticles. To date, very little is known about the prevailing reaction mechanism of this type of photoreaction. Here we provide a detailed study of the shape transformation dynamics as a function of a range of different process parameters, such as photon energy and photon flux. For the first time, we provide direct evidence that the photochemical synthesis of silver nanoprisms from spherical seed nanoparticles proceeds *via* a light-activated two-dimensional coalescence mechanism. On the other hand, we could show that Ostwald ripening becomes the dominant reaction mechanism when larger silver nanoprisms are grown from photochemically synthesized smaller nanoprisms. This two-step reaction proceeds significantly faster and yields more uniform, sharper nanoprisms than the classical one-step photodevelopment process from seeds. The ability to dynamically control nanoparticle shapes and properties with light opens up novel synthesis avenues but also, more importantly, allows one to conceive new applications that exploit the nonstatic character of these nanoparticles and the ability to control and adjust their properties at will in a highly dynamic fashion.

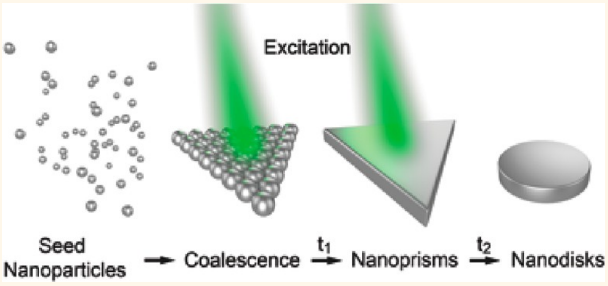

KEYWORDS: silver nanoparticles · wavelength-dependent growth · induction time · photo-oxidation · photoablation · coalescence

Due to their unique optical properties, metal nanoparticles have found applications in a wide array of technologies such as solar cells,[1,2] biosensors,[3,4] and photocatalysis.[5,6] A number of chemical synthesis techniques are known to produce metal nanoparticles with a variety of shapes and sizes.[7−13] The commonly used seed-mediated synthesis method is a two-step process. First, small (∼4−10 nm) metal nanoparticles (seeds) are formed through the chemical reduction of metal ions in the presence of stabilizing agents.[14] Subsequently, these seed particles are grown into anisotropic shapes by the addition of further reducing agents. Neither of the two processes is light-driven. Photochemical synthesis routes represent an exciting alternative to classical synthesis methods.[15] Previously, a range of photochemical synthesis strategies have found merit in the synthesis of metal nanoparticles, yielding a variety of distinct shapes such as nanoprisms, nanobipyramids, nanodisks, nanorods, and nanohexagons.[16−21] Despite the large number of photochemical synthetic strategies reported, it is still not known how electromagnetic radiation throughout the visible region guides the growth process of silver particles. The decay of a plasmonic excitation is believed to result in the formation of a hot electron−hole pair.[22,23] A hot hole transfer follows this process to a surface-adsorbed reducing agent such as citrate. The excess electron then reduces a silver ion in solution, resulting in nanoparticle growth.[22]

* Address correspondence to udo.bach@monash.edu.

Received for review March 14, 2013 and accepted June 3, 2013.

Published online June 03, 2013
10.1021/nn4013059

© 2013 American Chemical Society

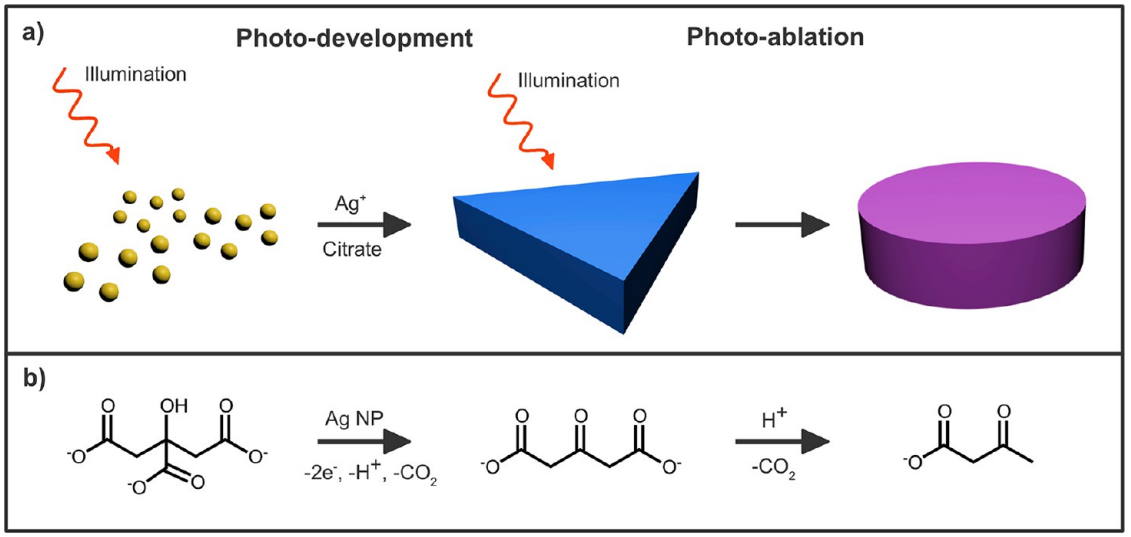

Scheme 1. (a) Schematic illustration of the photoinduced conversion of AgNP seeds to Ag nanoprisms in the presence of citrate that acts as a surfactant and a photoreducing agent and their subsequent photoablation to disk-shaped AgNPs upon prolonged illumination. (b) Mechanism of photochemical citrate oxidation in the presence of AgNPs.

Mirkin's research group was first to report on the light-mediated formation of Ag nanoprisms from spherical seed particle solutions in the presence of citrate as a reducing agent and shape-directing surfactant.[24] The sizes of these as-synthesized prisms increased linearly with the excitation wavelength used in the photodevelopment process.[24,25] Upon prolonged exposure, the initially formed prism-shaped nanoparticles were observed to transform to disk-shaped nanoparticles in a photoablation process (Scheme 1a).[20] The onset of the photoablation process has been explained on the basis of citrate depletion from the reaction solution due to its continuous photo-oxidation.[20] In the presence of citrate, the nanoprisms are protected against photocorrosion, due to the formation of a protective citrate monolayer on the prisms' [111]-type facets. Citrate also fills hot charge carrier vacancies in the nanoparticle *via* a sacrificial electron donation process (Scheme 1b).[20,26]

Here we aim to elucidate the mechanisms responsible for the light-driven development and ablation of silver nanoprisms and to identify significant process parameters, which predetermine the properties of the resulting metal nanoparticles.

RESULTS AND DISCUSSION

Wavelength Dependence and Temporal Evolution. The reaction dynamics as well as the final shapes and sizes of the nanoparticles strongly depend on the wavelength of light used in the photodevelopment process. Figure 1 illustrates the temporal evolution of different nanoparticle shapes and their corresponding absorption spectra during a typical citrate-mediated photodevelopment process. Blue (445 nm), green (503 nm), and orange (593 nm) color light was used for the photoexcitation of the nanoparticle solutions. The light intensity of all three light sources was adjusted to yield an identical photon flux of 1.5×10^{18} photons cm^{-2} s^{-1}. The position and number of surface plasmon resonance bands (SPRBs) observed in Figure 1 contains important information about the shapes and sizes of the AgNPs.[27] The initial seed nanoparticles have a single dipole absorption band (blue spectra) at ~390 nm, as previously reported.[24] As the spherical seed nanoparticles photodevelop into prisms, a second absorption peak emerges. This peak is red-shifted from the initial peak and can be attributed to the in-plane dipole and in- and out-of-plane quadrupole SPRBs of the prism-shaped nanoparticles.[28] The in-plane dipole SPRB is the strongest absorbing feature in the spectra. The position of the emerging in-plane dipole SPRB depends on the excitation wavelength and red shifts with increasing excitation wavelength. This red shift is due to an increase in the average nanoprism size (Figure 1b,e,h), in accordance with previous studies.[25] Further illumination eventually results in the photoablation of the prisms to disk shapes, which results in a blue shift of the SPRBs (green spectra). The transformation of the prisms to disks has been reported to result from the photo-oxidation of Ag at the prism tip corners.[29] In agreement with the change in absorption characteristics, the TEM insets also show that the final size of the resulting disks increases with increasing excitation wavelength.

In an experiment in which the same photon flux of 1.5×10^{18} photons cm^{-2} s^{-1} was chosen for all excitation wavelengths, it was found that the reaction kinetics of the photodevelopment process systematically become faster with decreasing excitation wavelength. To better understand this phenomenon, we monitored the UV−vis spectra of the developing AgNP solutions at regular intervals during photodevelopment and photoablation (Figure 2). This was performed

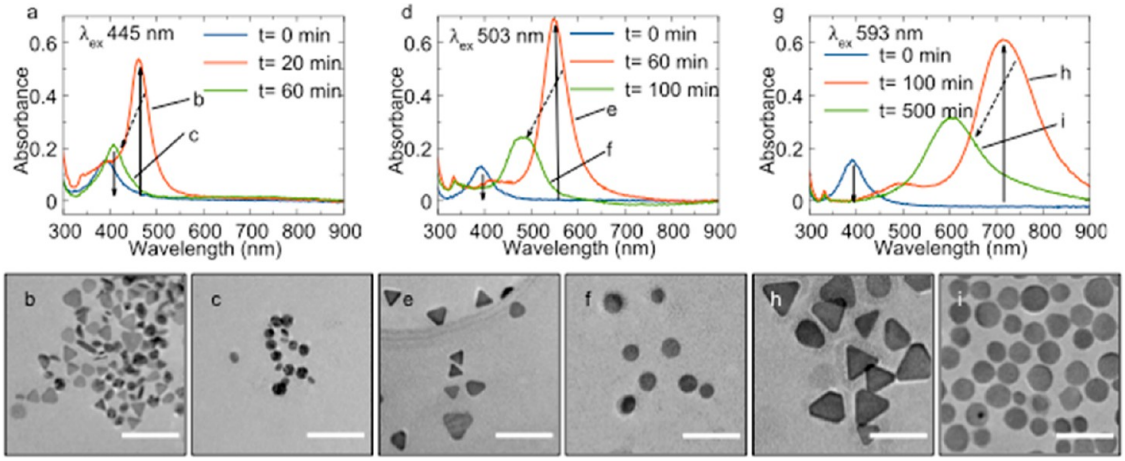

Figure 1. Properties of silver nanoparticles following photodevelopment and photoablation. Absorption spectra recorded for AgNP solutions photodeveloped at different excitation wavelengths: (a) 445 nm; (d) 503 nm, and (g) 593 nm). UV−vis spectra of the original seed AgNP solution (blue), photodeveloped silver nanoprism (red), and photoablated silver nanodisk (green) solutions are shown. Representative TEM micrographs of the respective photodeveloped (b,e,h) and photoablated nanoparticles (c,f,i) are also shown. All three photodevelopment reactions were performed under identical excitation photon flux conditions (1.5×10^{18} photons cm^2 s^{-1}). All scale bars in the TEM micrographs are equal to 100 nm.

for six different excitation wavelengths (λ_{ex}) in the range from 445 to 619 nm under identical photon flux conditions. Figure 2 shows the observed spectral reaction dynamics as contour plots. The spectral dynamics show a number of common features that are independent of the excitation wavelength. At the start of the photochemical reaction, the typical SPRB absorption of the seed particles can be observed with an absorption maximum at around ~390 nm. This absorption feature subsequently vanishes as a new SPRB emerges at wavelengths that are slightly longer than the excitation wavelength (shown as the white dotted line). Once established, this new SPRB only undergoes minor spectral changes over a prolonged period of time, until the abrupt onset of photoablation, which is witnessed as a spectral blue shift of the SPRB. The spectral features of the photoablated nanoparticles remain unchanged upon further illumination (see Supporting Information Figure S1).

Table 1 summarizes the results of a quantitative analysis of the reaction dynamics shown in Figure 2, combined with a TEM-based size analysis of the particles resulting from photodevelopment and photoablation. The appearance of the new SPRB was observed following an induction period that varied from 1 min for the shortest wavelength (445 nm) up to 47 min for longest wavelength used here (619 nm). This onset was accompanied with the simultaneous disappearance of the SPRB of the initial seed particles. Interestingly, during the longer induction phases, an increase in the absorption and width of the SPRB associated with the seed nanoparticles could be observed. The rate of change of absorption at the absorption maximum of the emerging SPRB ($(dAbs_{\lambda max}(t)/dt)_{max}$) is 1 order of magnitude faster for photodevelopment with short-wavelength light (445 nm), compared with longer wavelength photoexposure (619 nm). As observed in Figure 2, the solution illuminated with an excitation wavelength of 445 nm completed the growth and photoablation processes after 23 min. Whereas at 619 nm (λ_{ex}) photodevelopment set in only after an induction period of 47 min, photoablation only became apparent after more than 6 h of continuous illumination. The rate constants for photoablation again proved to be more than 1 order of magnitude faster for shorter wavelength excitation light. A similar trend was observed for the photodevelopment process (Table 1).

Phototransformation of Seeds to Nanoprisms. In the following, we aim to elucidate the hitherto mostly unexplored mechanism that leads to the photoinduced formation of prism-shaped silver nanoparticles. The photochemical reduction method has been reported to yield the abrupt appearance of prismatic nanoparticles in the early stages of photodevelopment.[30,31] Ostwald ripening[23] and coalescence[31] of seed particles were both postulated as possible mechanisms for the observed formation of prism-shaped AgNPs under illumination. Yu *et al.* were the first to provide evidence that the synthesis of silver nanoprisms in the absence of light, following the wet-chemical reduction method, proceeds *via* a combination of coalescence and dissolution−recrystallization mechanisms.[32] These mechanisms were also found to prevail during the electron-beam-induced formation of noble metal nanoparticles when observed in an *in situ* transmission electron microscope.[32] Furthermore, detailed studies conducted by the Huang research group elegantly demonstrated that Au nanoparticle coalescence of seed nanoparticles has been observed for the formation of nanoplates and octahedral shapes being induced by thermal and halogen methods.[33,34]

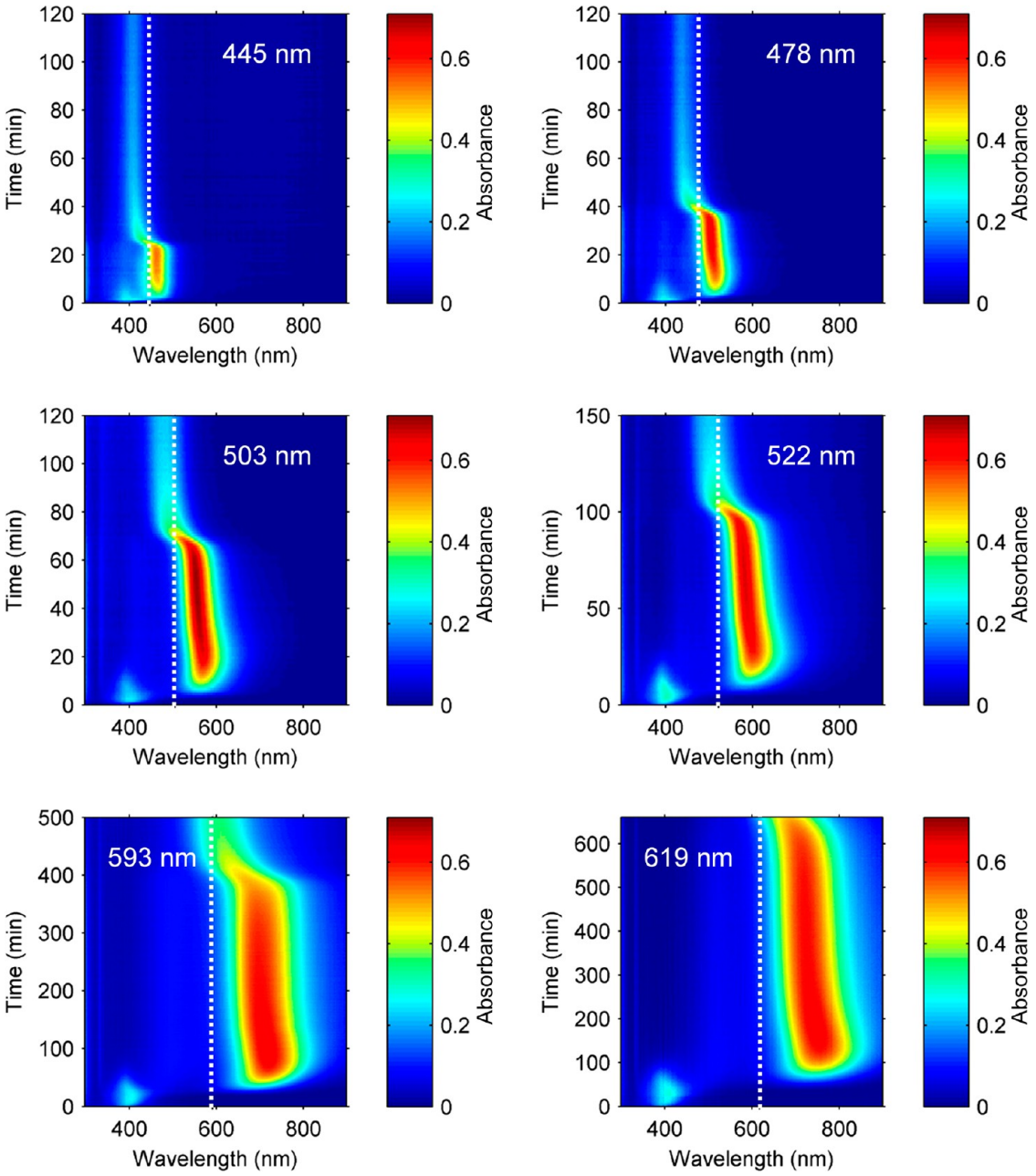

Figure 2. Time-dependent contour plots of the absorbance spectra of Ag nanoparticle solutions during illumination. The wavelength of light used for the photodevelopment is shown in each graph (white numbering and white dashed line). The photon flux was 1.5 × 10^{18} photons cm^{-2} s^{-1}.

In this study, a number of independent observations provide evidence for a light-driven nanoparticle growth mechanism based on two-dimensional particle coalescence. Figure 3 shows TEM images of AgNPs isolated from a photoinduced growth reaction at λ_{ex} of 619 nm immediately after the induction period (t_{ind}). Figure 3a shows transmission electron micrographs of nanoparticles, which already exhibit prismatic shapes similar to those found in completely photodeveloped particles but still reveal the granular structure of the seed AgNPs from which they were formed. Figure 3b–e shows partially formed nanoprisms in various development stages that provide strong evidence that coalescence of seed AgNPs is the dominant mechanism in the light-driven growth process of silver nanoprisms from seeds. Like the previously reported thermally induced coalescence from seed nanoparticles, many of the nanoparticles are fused toward the central regions to form a thick mass.[33] The spectral dynamics in Figure 2 show a spontaneous evolution of the prism SPRB, accompanied by a simultaneous disappearance of the SPRB of the initial seed nanoparticles. This also points to a coalescence process rather than Ostwald ripening as the underlying mechanism for nanoprism growth. Interestingly, the sizes of the coalesced aggregates appear larger than the final nanoprisms, pointing toward

TABLE 1. Influence of the Excitation Wavelength (λ_{ex}) on Reaction Dynamics and Silver Nanoparticle Properties[a]

	photodeveloped					photoablation				
λ_{exc} (nm)	t_{ind} (min)	(dAbs/dt) (Abs)	λ_{max} (nm)	fwhm (eV)	size (nm)	$t_{ablation}$ (min)	(dAbs/dt) (Abs)	λ_{max} (nm)	fwhm (eV)	size (nm)
445	1.0	0.138	462	0.30	19 ± 6	22.7	−0.128	407	0.44	14 ± 4
478	1.3	0.116	504	0.27	21 ± 4	34.1	−0.106	433	0.46	15 ± 3
503	2.8	0.074	553	0.27	28 ± 7	64.8	−0.046	476	0.45	21 ± 5
522	4.8	0.033	583	0.30	35 ± 9	95.7	−0.031	504	0.46	26 ± 6
593	24.0	0.024	712	0.34	51 ± 8	373	−0.010	609	0.45	36 ± 8
619	47.0	0.013	767	0.36	59 ± 7	N/A	N/A	N/A	N/A	N/A

[a] The time-dependent spectral evolution data shown in Figure 2 was analyzed to retrieve the following parameters: the induction times (t_{ind}) and ablation times ($t_{ablation}$) corresponding to the overall reaction times that lapsed before the onset of photodevelopment and photoablation were observed (see Supporting Information Figure S2). The maximum rate of absorbance change (dAbs/dt) for the appearance and disappearance of the nanoprism SPRB (at λ_{max}) during photodevelopment and photoablation, respectively, were determined from the time derivative of the $Abs_{\lambda max}(t)$ curve. Full width at half-maximum (fwhm) of the surface plasmon resonance band of photodeveloped and photoablated AgNPs and the nanoparticle sizes of photodeveloped and photoablated nanoparticles, as determined from TEM analysis. The photon flux was kept constant at 1.5×10^{18} photons cm^{-2} s^{-1} for each experiment.

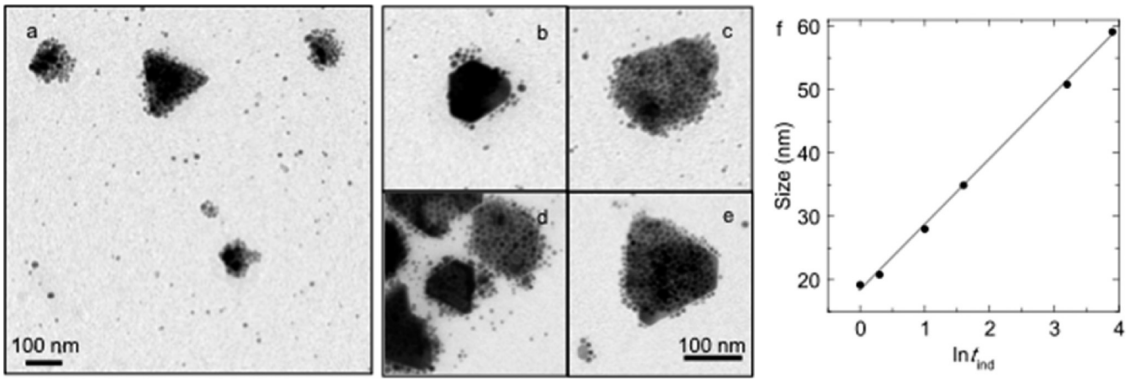

Figure 3. Transmission electron micrographs. (a−e) TEM images of nanoparticles sampled from a photodevelopment process after 47 min (t_{ind}) of illumination at 619 nm. Different stages of light-activated seed particle coalescence can be seen ranging from an early stage cluster formation to nanoparticles that already exhibit prism-like shapes. (f) Plot of the size of the photodeveloped silver nanoprisms obtained from TEM analysis as a function of the natural logarithm of the observed induction time for the photodevelopment measured at different excitation wavelengths (λ_{ex}) and a photon flux of 1.5×10^{18} photons cm^{-2} s^{-1}. (b-e) Same scale bar.

subsequent additional transformation modes that lead to the final crystalline structure. A growth process based on Ostwald ripening would result in a continuous spectral shift of the original seed nanoparticles' SPRB as their sizes change gradually. However, this is not observed experimentally: SPRBs of AgNPs of intermediate sizes (between seed particle and the final prism size) could not be identified in any of the absorption spectra obtained during the photodevelopment process (Figure 2). TEM analysis of aliquots taken from the reaction solution prior to t_{ind} showed no evidence of nanoparticle coalescence.

The observed excitation wavelength dependence of the induction time can provide additional indications toward the underlying growth mechanism. While induction times to date have not been analyzed for the light-induced formation of silver nanoprisms, Ghader *et al.* have studied induction times for the wet-chemical synthesis of spherical silver nanoparticles in the absence of light to investigate the underlying growth mechanism.[35] The driving force for assembling the seed nanoparticles into nanoplates is unclear. Assuming a thermally activated crystallization process in which the rate-limiting step is the nucleation of a particle cluster of a critical size, the induction time (t_{ind}) depends on the free energy barrier to nucleation (ΔG_c) according to the Arrhenius relationship:[36]

$$t_{ind} = A\exp\left(\frac{\Delta G_c}{k_B T}\right) \quad (1)$$

In this equation, A is an kinetic prefactor,[37] k_B is the Boltzmann constant, and T is the absolute temperature (temperatures during the experiment were found to vary slightly (3 K) depending on the light source used and were found to have an insignificant affect on the experiment, Figure S3). We propose that the formation of prismatic AgNPs from seed particles can be described as such a two-dimensional crystallization process. The hypothesis that the observed nanoparticle growth is essentially two-dimensional is supported by a strong correlation between the observed prism z-height (9 ± 2 nm) and the size of the original seed

particles (10 ± 3 nm): seed particles assemble and crystallize in only two dimensions to form prisms. Furthermore, all photodeveloped prisms are of the same *z*-height independent of their size (ranging from 19 to 59 nm in bisector length), which also emphasizes the two-dimensionality of the underlying process.

Following classical nucleation theory and assuming that the free energy change associated with the coalescence of seed particles to form a prismatic nanoparticle is a sum of bulk and surface terms,[32,33] the free energy activation barrier for nucleation (ΔG_c) can be shown to be related to the critical particle size L_c at the barrier by

$$\Delta G_c = \frac{Ch\gamma}{2} L_c \qquad (2)$$

where γ is the interfacial tension between the prism's growth faces and the solution, h is the height of the prism, and C is a dimensionless geometric factor defined such that CL_c is the prism's circumference around the growth faces (see Supporting Information for details). ΔG_c is also directly proportional to the particle size $L_0 = 2L_c$ at which the prisms become more stable than the seed particles.

Thus, for an anisotropic crystallization process that follows eqs 1 and 2, we expect a linear relationship between $\ln(t_{ind})$ and the nanoparticle size. Figure 3f illustrates that the nanoparticle size does indeed increase linearly with $\ln(t_{ind})$, supporting the hypothesis that the light-driven development of silver nanoparticles proceeds *via* an anisotropic two-dimensional crystallization process.

Another possible explanation for the observed growth pattern is an autocatalytic process. Here the formation of prism Ag particles would be catalyzed by the presence of previously formed nanoprisms. To test this hypothesis, a control experiment was conducted, in which a small volume (2%) of a fully developed nanoprism solution was added to a freshly prepared seed solution prior to its photodevelopment. As indicated in Figure 4a,b, the presence of preformed nanoprisms does not affect the duration of the induction phase, so that an autocatalytic mechanism can clearly be ruled out.

Growing Large Nanoprisms from Smaller Ones. In a separate study, we investigated whether preformed smaller nanoprisms can be used as building blocks to grow larger nanoprisms by exploiting the same coalescence mechanism as described above. In this experiment, we first used a 503 nm (λ_{ex}) to grow silver nanoprisms from seed particles for 20 min and then switched to a 619 nm (λ_{ex}) for an additional 20 min to grow bigger nanoprisms. The spectral reaction dynamics during this dual wavelength photodevelopment experiment are shown in Figure 4c. The spectral evolution observed during the first 20 min of 503 nm (λ_{ex}) is identical to the data presented for the single wavelength photodevelopment process (see Figure 2) under 503 nm (λ_{ex}) illumination. When the excitation wavelength is changed from 503 to 619 nm (λ_{ex}), the initially formed SPRB, centered around 560 nm, blue shifts abruptly and disappears gradually. Simultaneously, a new SPRB emerges from the spectral position of the originally formed SPRB, which continuously red shifts and increases in absorption over time, stabilizing at about 680 nm (see Supporting Information Figure S4).

To further elucidate the dominant growth mechanism in this experiment, aliquots of the reaction solution were taken at different reaction times (20, 22, 27, and 40 min) and analyzed by transmission electron microscopy. The results illustrated in Figure 4d,e show that the predominant nanoparticle size yielded after the first 20 min of 503 nm (λ_{ex}) illumination is 23 to 29 nm. Two minutes after the wavelength was changed over, the relative frequency of occurrence of these particle sizes is decreased, both in favor of smaller (19 nm) *and* larger (32 nm) nanoparticles. Furthermore, TEM images reveal an increased occurrence of growing nanoprisms and shrinking nanodisks over this 2 min period. Upon further 619 nm (λ_{ex}) illumination (7 min total), the average size distribution broadens and shifts to larger nanoparticles. At this stage, the sizes of the nanoprisms are again observed to increase. After 20 min of photodevelopment with the 619 nm (λ_{ex}), the majority of the particles are nanoprisms with a minority of small spherical nanoparticles observed (Figure 4e(iv)). The full width at half-maximum of the final SPRB at ~678 nm was 0.22 eV. TEM micrograph image analysis of the nanoparticles shows that the size distribution of the alternate dual excitation wavelength synthesis method produces nanoparticle sizes with a narrower size distribution at the half-width of the histogram (14.5 nm) compared to that of the single excitation wavelength method (18.1 nm) (see Supporting Information Figure S5). Additionally, two distinct populations of sizes are observed in the histograms of the alternate dual excitation wavelength synthesis method.

The continuous transition from one SPRB band to another in the absorption characteristics as well as the TEM analysis of the corresponding NP sizes suggests that the process underlying the growth from medium sized (~26 nm) to large prisms (32 nm) in this experiment is Ostwald ripening rather than coalescence. When the excitation wavelength is changed, one part of the medium sized prism population *shrinks* and thereby donates silver ions to the further growth of the other part of the population. Both shrinking and continuous further growth of the medium sized NPs can be clearly identified in the absorption spectra (Figure 4c): the blue shift and successive disappearance of the medium sized prism's SPRB (shrinking); the red shift and gradual increase of the same SPRB (further growth) at the time of excitation wavelength changeover.

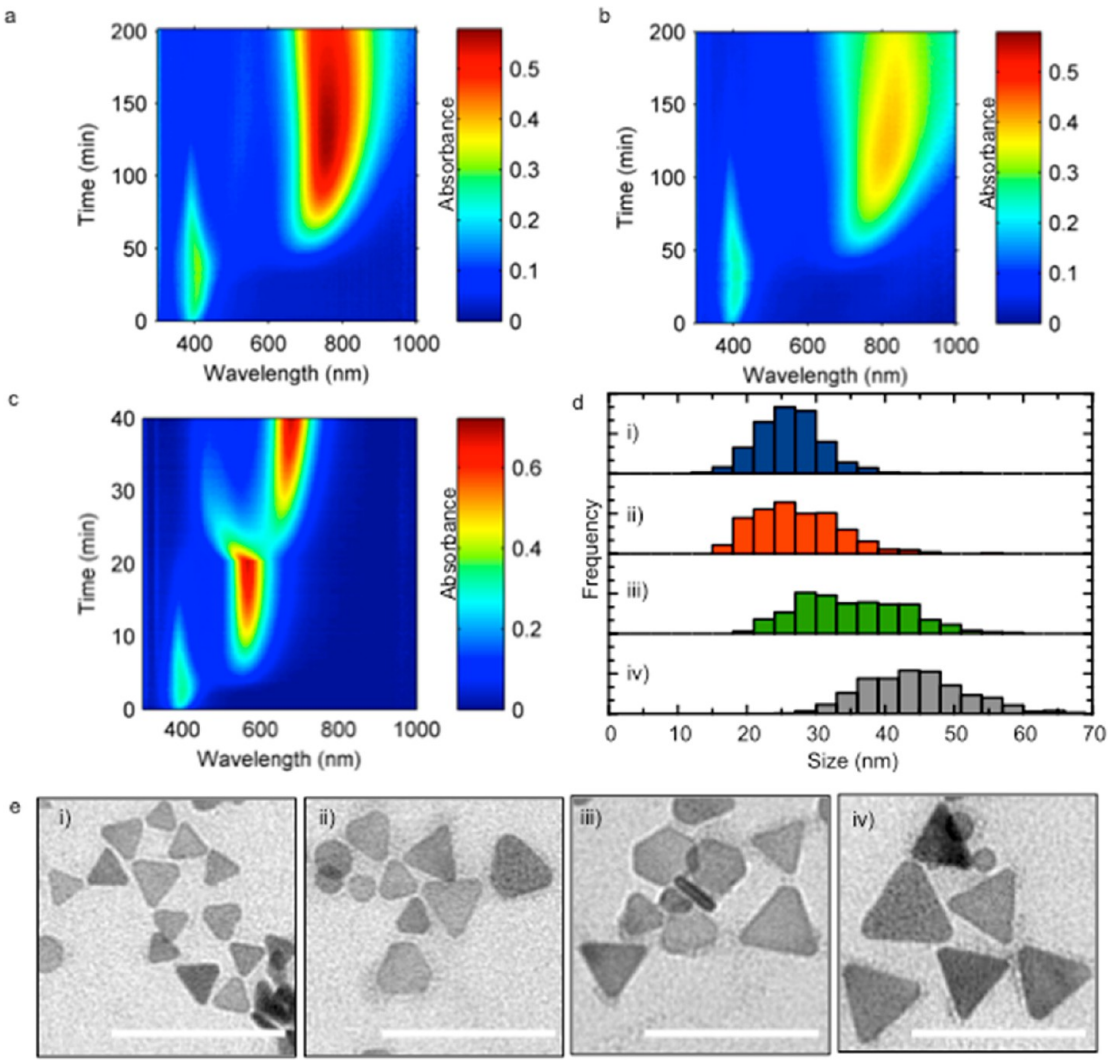

Figure 4. Comparison of different photodevelopment experiments. (a) Absorption spectra contour plot of a typical seed AgNP solution that was photoilluminated for 200 min (λ_{ex} = 619 nm). (b) Absorption spectra contour plot for the evolution of a seed AgNP solution that was spiked with (2%) preformed nanoprisms and photodeveloped for 200 min (λ_{ex} = 619 nm). (c) Absorption spectra contour plot of a seed AgNP solution that was initially photoilluminated using 503 nm (λ_{ex}) for 20 min followed by a subsequent photoillumination using 619 nm (λ_{ex}) for an additional 20 min. All solutions were photoilluminated using a photon flux of 1.7 $\times$ 10^{18} photons cm^{-2} s^{-1}. (d) Histogram* of the frequency *versus* size (bisector length) distribution and representative TEM images of the silver nanoprisms (e) at different stages of the dual wavelength photodevelopment experiment: (i) after 20 min of 503 nm (λ_{ex}) illumination as well as an additional (ii) 2, (iii) 7, and (iv) 20 min of 619 nm (λ_{ex}) illumination. All scale bars in the TEM micrographs are equal to 100 nm. *Bin size = 3 nm; nonprismatic nanoparticles were not included in the statistical analysis; *n* = 2000 nanoparticles.

The mechanistic transition from nanoparticle growth by seed particle coalescence to growth by Ostwald ripening is due to a combination of factors. First, the absence of seed particles following the initial 503 nm (λ_{ex}) illumination eliminates the coalescence pathway during the subsequent 619 nm (λ_{ex}) illumination step. Second, most the nanoprisms formed from the initial illumination are likely postcritical nuclei, whereas the seed particles are likely precritical with respect to the solution; thus, whereas nucleation of larger nanoparticles *via* growth of seed particles appears to be inhibited by a high activation barrier, this barrier is absent in the case of nanoprism growth, allowing the latter mechanism to dominate during the subsequent illumination step. Furthermore, although most of the nanoprisms appear to be postcritical nuclei in the second illumination step, the observation of two distinct populations of sizes following this second step suggests that the smaller nanoprisms in the tail of the size distribution after the first illumination step are precritical: in the second illumination step, most of the prisms grow in size *via* Ostwald ripening at the expense of these smaller prisms, which in turn shrink, resulting in the two populations of particle sizes that are observed.

Generally, for the successful light-driven synthesis of silver nanoprisms, we observed that the age of the seed solutions and the overall photon flux are critical reaction parameters. The height and half-width of the

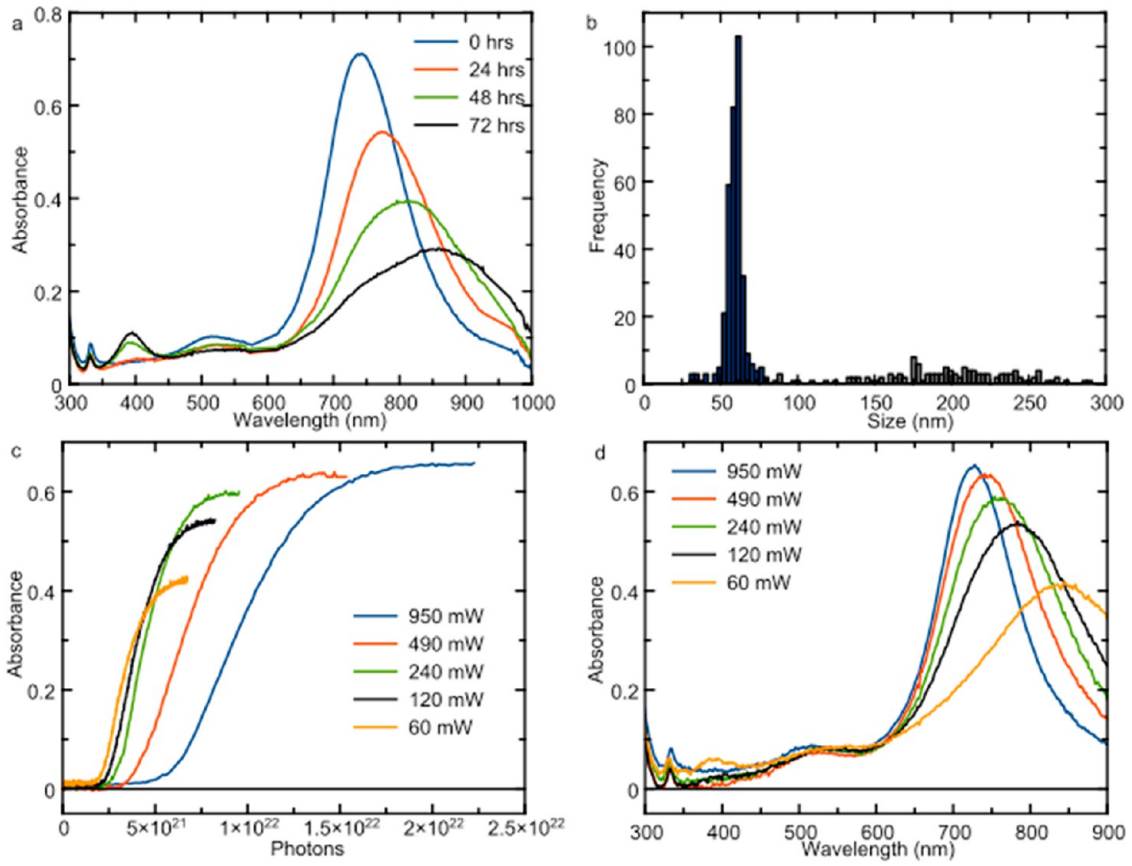

Figure 5. Influence of seed solution aging and photon flux on the photodevelopment process. (a) UV−vis spectra of AgNP solutions that were photodeveloped for 80 min (λ_{ex} = 619 nm) after the initial seed solutions were aged for 0, 24, 48, and 72 h. (b) Histogram of nanoparticles *versus* prism bisector length (bin sizes of 3 nm, n = 476) for the solutions that underwent photodevelopment after initial synthesis (blue) and aged in the dark for 72 h (gray) prior to photodevelopment. Each solution was photodeveloped for 80 min with an identical photon flux of 2.2 × 10^{18} photons cm^{-2} s^{-1}. (c) Absorbance values at λ_{max} of solutions photodeveloped with an excitation wavelength of 619 nm at different light intensities as a function of the accumulated number of incident photons. (d) Absorption spectra of Ag nanoprisms developed at different light intensities. The photon fluxes used were 0.19, 0.37, 0.75, 1.5, and 3.0 × 10^{18} photons cm^{-2} s^{-1}.

SPRB provides a good indication of the yield and monodispersity of the resulting nanoprisms. Storing a freshly prepared AgNP seed solution for 24, 48, and 72 h in the dark at room temperature prior to the actual photodevelopment step resulted in a significant reduction in the maximum absorption of the SPRB as well as a remarkable increase in peak half-width, indicating a broadening of the size distribution (Figure 5a). This was accompanied with a significant red shift of the SPRB, indicative of an increase in the average nanoparticle size, which was verified by TEM image analysis. Developing a freshly prepared seed solution yielded silver nanoprisms of a very uniform size (59 ± 7 nm). When photodeveloped from a seed solution that had been stored for 72 h, the average size of the silver nanoprisms increased to 132 ± 72 nm (Figure 5b). The average *z*-height of the nanoparticles in a solution aged for 72 h was 18 ± 4 nm. This reveals that the final nanoprism size is not exclusively predetermined by the excitation wavelength but also depends on the nature of the seed particles. Using a zeta particle sizer, we were able to observe an increase in the hydrodynamic diameter of the seed nanoparticles from 10 ± 1 to 17 ± 1 nm, 19 ± 3, and 19 ± 2 nm as the seed particles aged for 0, 24, 48, and 72 h. The fact that the *z*-height of 18 ± 4 nm of the prisms photodeveloped from the 72 h aged seed solution again is equal to the diameter of the seeds of the aged solution (19 ± 2 nm) is further evidence for a two-dimensional coalescence process. The photon flux used for photodevelopment appeared to have a similar effect on the quality of the resulting nanoprisms. As the photon flux increases, smaller nanoprisms with a more monodisperse size distribution are obtained. Interestingly, we observed a nonlinear dependence between the induction time and the photon flux (Figure 5c). When plotting the absorption of the AgNP solution at λ_{max} of the photodeveloped nanoprisms against the accumulated number of incident photons, we observe that nanoprism growth can be induced with a smaller number of incident photons at lower photon fluxes (Figure 5c). Also, the absorption spectra of prismatic silver nanoparticles photodeveloped at different light intensities show a pronounced red shift of the absorption maximum as light intensities decrease (Figure 5d).

CONCLUSIONS

The light-driven citrate-mediated synthesis of AgNPs from initial seeds to prism shapes and their subsequent photoablation to disks was investigated. We observed that the reaction dynamics strongly depend on the excitation wavelength and the photon flux used to drive the reaction, affecting the onset times for photodevelopment and photoablation. For the first time, we provide direct evidence that the growth of silver nanoprisms from seed AgNPs proceeds *via* a coalescence process that involves the aggregation of seed AgNPs to final prism shapes. The linear dependence between the natural logarithm of the induction time and the size of the resulting nanoprisms indicates the prevalence of an activated 2D growth process that obeys the Arrhenius reaction velocity relationship. Autocatalytic mechanisms for nanoprism growth could be excluded. The sizes of the original seed nanoparticles as well as the overall photon flux are critical reaction parameters that determine the quality of the photodeveloped silver nanoprism solutions. Highly monodisperse solutions of nanoprisms were obtained at high yields when the photodevelopment was performed with fresh AgNP seed solutions at high photon fluxes. An increased reaction rate for nanoprisms was demonstrated when the excitation wavelength was changed during photodevelopment and a decreased full width at half-maximum of the surface plasmon resonance band was observed. Ostwald ripening of intermediately formed smaller silver nanoprisms was found to be the prevailing reaction mechanism for the second phase of the two-step photoreaction. The present study yields important insight into the mechanism of a classical light-driven metal nanoparticle growth process while also providing an overview over the major parameters affecting the quality of the resulting metal nanoparticles. This highlights the great potential of controlling the size and shape of matter on the nanoscale in a single reaction vessel simply by controlling the illumination conditions.

In contrast to most classical colloidal synthesis routes, nanoparticles yielded from photomorphic reactions, once synthesized, retain their susceptibility to external stimulus, such as light, to respond with changes to their sizes and shapes. This has important implications in areas such as nanoparticle synthesis, such as for the growth of metallic nano-heterostructures and medicine, such as the development of agents for photodynamic therapy.

METHODS AND MATERIALS

Formation of Seed Nanoparticles. Seed AgNPs, used for photodevelopment, were synthesized using a wet-chemistry technique as reported previously by sequentially combining 1.0 mL of 0.005 M $AgNO_3$, 1.0 mL of 0.02 M trisodium citrate, 1.0 mL of 0.02 M $NaBH_4$, and 1.0 mL of 0.005 M 4,4′ (phenylphosphinidene) bis(benzenesulfonic) acid dipotassium salt (BSPP) to 96.0 mL of H_2O while stirring.[29] All stock solutions and experiments used reverse osmosis water as the solvent. These as-synthesized seed solutions were sealed with parafilm and allowed to rest in the dark for a minimum of 30 min before photodevelopment with a high-intensity LED light source (Luxeon Star, Canada, see below). The seed solutions underwent photodevelopment using 2 mL volumes in 3.5 mL plastic cuvettes and were photodeveloped for varying lengths of time. Fresh seed solutions (within 1 h of preparation) were used in these reported experiments unless stated otherwise. Prior to the synthesis, all glassware was thoroughly washed with 2 M HNO_3 followed by six rinses with water. Then, the glassware was allowed to completely dry overnight.

Light Sources. High-intensity LED arrays (containing 7 high-power LEDs) were equipped with a narrow focus cluster lens (Polymer Optics; part number 263). The LEDs featured narrow emission profiles (spectral half-width = 30−80 nm), and emission maxima were determined ranging from 445 to 619 nm: royal blue [445 nm] (SR-02-R0500), blue [478 nm] (SR-02-B0030), cyan [503 nm] (SR-02-E0070), green [522 nm] (SR-02-M0100), red [593 nm] (SR-02-D2050), and deep red [619 nm] (SR-02-D3350) (see Supporting Information for the emission profiles; Figure S6). (Warning: these light sources are very bright, reaching several times the intensity of the sun at their focal point. This is potentially damaging to the eye. Proper protective equipment and encasement of the experiment is necessary.)

LED Setup and UV−Vis Measurements. The setup of the LEDs was done by aligning and focusing the focal point of the LEDs to the bottom of the 1 cm^2 cuvettes (see Supporting Information Figure S7). Importantly, the cuvettes were sealed by parafilm to prevent evaporation. Additionally, a cuvette cover was used to secure the photodeveloping solutions. The cuvette containing the solution was housed in an Ocean Optics (HR-4000) cuvette holder (Ocean Optics, USA). The beam height of the Ocean Optics spectrophotometer is 15 mm, measured from of the bottom of the cuvette. The LED arrays were connected to a DC power supply (0−60 V, 0−1 A) (Iso-Tech, Australia). The LED arrays were switched off for the time that spectra were collected (2 s).

Constant Photon Flux Experiment. To compare the effect of excitation wavelength on the dynamics of the photodevelopment process, a series of experiments were conducted at different wavelengths. For these studies, the current input to the LEDs was adjusted to yield a set photon flux that was equal for all photodevelopment processes independent of excitation wavelength. A thermophile (Thorlabs, model 310C) was used to determine the energy output of the LEDs. A 1 cm × 1 cm mask was placed directly over the cavity of the sensor (which was the dimensions of the well that the cuvettes occupied during photodevelopment). The beam of the LED was focused on the inside area of the opening of the mask. The average photon energy was calculated based on the LED emission profile (see Supporting Information Figure S6). The thermophile was allowed to stabilize for approximately 30 min, and the input current of the LED was then slowly adjusted until the values plateaued at the required output energy (photon flux) for the experiment. The LEDs were used at different photon fluxes ranging between 0.19 and 3.0 × 10^{18} photons cm^{-2} s^{-1}. For reference, the solar photon flux below 1000 nm at the surface of the earth is 4.3 × 10^{17} cm^{-2} s^{-1} for the entire AM 1.5 G spectrum with 1000 W m^{-2}.

Preparation of TEM Grids and the Shape Passivation of the AgNP Solutions. We observed early during our experimental processing that AgNPs undergo shape changes during and after the deposition onto TEM grids. We observed that this shape transformation could be stopped through a surface passivation step that involved the addition of 3 μL of 0.005 M 1-phenyl-1*H*-tetrazole-5-thiol sodium salt (NaPTT) to 2 mL of the photodeveloped solutions. The chemisorption of the bidentate ligand NaPTT onto the silver surfaces has been reported in the literature, and we found it to be an excellent passivation agent for AgNPs, superior to more commonly reported alkanethiol

passivation agents.[38] The AgNPs were concentrated by centrifugation (5.9 rcf for 60 min). Then, the concentrated AgNPs were drop-casted onto 300 μm, carbon-coated Cu grids (Ted Pella Inc., USA) and allowed to dry for several hours in the dark. Approximately, 6000 nanoparticles were characterized by TEM image analysis (400 spherical seeds, 4459 photodeveloped prisms, and 850 photoablated disks) using ImageJ software.[39]

Conflict of Interest: The authors declare no competing financial interest.

Acknowledgment. This research used equipment funded by Australian Research Council grants (AL9132708 and RIEFP 99). The authors acknowledge use of the facilities at the Monash Centre for Electron Microscopy. The authors acknowledge financial support from the Australian Research Council through an Australian Research Fellowship (U.B.). Further financial support has been received from Commonwealth Scientific and Industrial Research Organization through an OCE Science Leader position (U.B.). This work was performed in part at the Melbourne Centre for Nanofabrication, an initiative partly funded by the Commonwealth of Australia and the Victorian Government.

Supporting Information Available: Characterization of LEDs, experimental setup and analysis methods, UV−vis spectra used for tabulated results, and derivation of equations used for the relationship between induction time and nanoparticle size. This material is available free of charge *via* the Internet at http://pubs.acs.org.

REFERENCES AND NOTES

1. Reineck, P.; Lee, G. P.; Brick, D.; Karg, M.; Mulvaney, P.; Bach, U. A Solid-State Plasmonic Solar Cell *via* Metal Nanoparticle Self-Assembly. *Adv. Mater.* **2012**, *24*, 4750–4755.
2. Atwater, H. A.; Polman, A. Plasmonics for Improved Photovoltaic Devices. *Nat. Mater.* **2010**, *9*, 205–213.
3. Haes, A. J.; Van Duyne, R. P. A Nanoscale Optical Biosensor: Sensitivity and Selectivity of an Approach Based on the Localized Surface Plasmon Resonance Spectroscopy of Triangular Silver Nanoparticles. *J. Am. Chem. Soc.* **2002**, *124*, 10596–10604.
4. Beeram, S. R.; Zamborini, F. P. Purification of Gold Nanoplates Grown Directly on Surfaces for Enhanced Localized Surface Plasmon Resonance Biosensing. *ACS Nano* **2010**, *4*, 3633–3646.
5. Beydoun, D.; Amal, R.; Low, G.; McEvoy, S. Role of Nanoparticles in Photocatalysis. *J. Nanopart. Res.* **2000**, *1*, 439–458.
6. Chen, X.; Zheng, Z.; Ke, X.; Jaatinen, E.; Xie, T.; Wang, D.; Guo, C.; Jincai, Z.; Huaiyong, Z. Supported Silver Nanoparticles as Photocatalysts under Ultraviolet and Visible Light Irradiation. *Green Chem.* **2010**, *12*, 414–419.
7. Dong, X.; Ji, X.; Wu, H.; Zhao, L.; Li, J.; Yang, W. Shape Control of Silver Nanoparticles by Stepwise Citrate Reduction. *J. Phys. Chem. C* **2009**, *113*, 6573–6576.
8. Siekkinen, A. R.; McLellan, J. M.; Chen, J.; Xia, Y. Rapid Synthesis of Small Silver Nanocubes by Mediating Polyol Reduction with a Trace Amount of Sodium Sulfide or Sodium Hydrosulfide. *Chem. Phys. Lett.* **2006**, *432*, 491–496.
9. Panfilova, E. V.; Khlebtsov, B. N.; Burov, A. M.; Khlebtsov, N. G. Study of Polyol Synthesis Reaction Parameters Controlling High Yield of Silver Nanocubes. *Colloid J.* **2012**, *74*, 99–109.
10. Cathcart, N.; Kitaev, V. Monodisperse Hexagonal Silver Nanoprisms: Synthesis *via* Thiolate-Protected Cluster Precursors and Chiral, Ligand-Imprinted Self-Assembly. *ACS Nano* **2011**, *5*, 7411–7425.
11. Lee, G.; Shin, S.; Kim, Y.; Oh, S. Preparation of Silver Nanorods through the Control of Temperature and pH of Reaction Medium. *Mater. Chem. Phys.* **2004**, *84*, 197–204.
12. Chen, E.; Su, H.; Zhang, W.; Tan, T. A Novel Shape-Controlled Synthesis of Dispersed Silver Nanoparticles by Combined Bioaffinity Adsorption and TiO_2 Photocatalysis. *Powder Technol.* **2011**, *212*, 166–172.
13. Yu, P.; Huang, J.; Yuan, C.-T.; Tang, J. Synthesis of Silver Nanoprisms and Nanodiscs an Applications in Fluorescence Blinking Suppression. *J. Chin. Chem. Soc.* **2010**, *57*, 528–533.
14. Chen, S.; Carroll, D. L. Synthesis and Characterization of Truncated Triangular Silver Nanoplates. *Nano Lett.* **2002**, *2*, 1003–1007.
15. Sakamoto, M.; Majima, T. Photochemistry for the Synthesis of Noble Metal Nanoparticles. *Bull. Chem. Soc. Jpn.* **2010**, *83*, 1133–1154.
16. Tang, B.; Xu, S.; An, J.; Zhao, B.; Xu, W. Photoinduced Shape Conversion and Reconstruction of Silver Nanoprisms. *J. Phys. Chem. C* **2009**, *113*, 7025–7030.
17. Zhang, J.; Langille, M. R.; Mirkin, C. A. Photomediated Synthesis of Silver Triangular Bipyramids and Prisms: The Effect of pH and BSPP. *J. Am. Chem. Soc.* **2010**, *132*, 12502–12510.
18. Maillard, M.; Huang, P.; Brus, L. Silver Nanodisk Growth by Surface Plasmon Enhanced Photoreduction of Adsorbed [Ag^+]. *Nano Lett.* **2003**, *3*, 1611–1615.
19. Zhang, J.; Langille, M. R.; Mirkin, C. A. Synthesis of Silver Nanorods by Low Energy Excitation of Spherical Plasmonic Seeds. *Nano Lett.* **2011**, *11*, 2495–2498.
20. Lee, G. P.; Bignell, L. J.; Romeo, T. C.; Razal, J. M.; Shepherd, R. L.; Chen, J.; Minett, A. I.; Innis, P. C.; Wallace, G. G. The Citrate-Mediated Shape Evolution of Transforming Photomorphic Silver Nanoparticles. *Chem. Commun.* **2010**, *46*, 7807–7809.
21. Sun, Y.; Xia, Y. Triangular Nanoplates of Silver: Synthesis, Characterization, and Use as Sacrificial Templates for Generating Triangular Nanorings of Gold. *Adv. Mater.* **2003**, *15*, 695–699.
22. Redmond, P. L.; Wu, X.; Brus, L. Photovoltage and Photocatalyzed Growth in Citrate-Stabilized Colloidal Silver Nanocrystals. *J. Phys. Chem. C* **2007**, *111*, 8942–8947.
23. Wu, X.; Redmond, P. L.; Liu, H.; Chen, Y.; Steigerwald, M.; Brus, L. Photovoltage Mechanism for Room Light Conversion of Citrate Stabilized Silver Nanocrystal Seeds to Large Nanoprisms. *J. Am. Chem. Soc.* **2008**, *130*, 9500–9506.
24. Jin, R.; Cao, Y.; Mirkin, C. A.; Kelly, K. L.; Schatz, G. C.; Zheng, J. G. Photoinduced Conversion of Silver Nanospheres to Nanoprisms. *Science* **2001**, *294*, 1901–1903.
25. Jin, R.; Cao, Y. C.; Hao, E.; Me, G. S.; Schatz, G. C.; Mirkin, C. A. Controlling Anisotropic Nanoparticle Growth through Plasmon Excitation. *Nature* **2003**, *425*, 487–490.
26. Seifert, G.; Stalmashonak, A.; Hofmeister, H.; Haug, J.; Dubiel, M. Laser-Induced, Polarization Dependent Shape Transformation of Au/Ag Nanoparticles in Glass. *Nanoscale Res. Lett.* **2009**, *4*, 1380–1383.
27. Aherne, B. D.; Ledwith, D. M.; Gara, M.; Kelly, J. M. Optical Properties and Growth Aspects of Silver Nanoprisms Produced by a Highly Reproducible and Rapid Synthesis at Room Temperature. *Adv. Funct. Mater.* **2008**, *18*, 2005–2016.
28. Sherry, L. J.; Jin, R.; Mirkin, C. a; Schatz, G. C.; Van Duyne, R. P. Localized Surface Plasmon Resonance Spectroscopy of Single Silver Triangular Nanoprisms. *Nano Lett.* **2006**, *6*, 2060–2065.
29. Lee, G. P.; Minett, A. I.; Innis, P. C.; Wallace, G. G. A New Twist: Controlled Shape-Shifting of Silver Nanoparticles from Prisms to Discs. *J. Mater. Chem.* **2009**, *19*, 8294–8294.
30. Millstone, J. E.; Hurst, S. J.; Métraux, G. S.; Cutler, J. I.; Mirkin, C. A. Colloidal Gold and Silver Triangular Nanoprisms. *Small* **2009**, *5*, 646–664.
31. Callegari, A.; Tonti, D.; Chergui, M. Photochemically Grown Silver Nanoparticles with Wavelength-Controlled Size and Shape. *Nano Lett.* **2003**, *3*, 1565–1568.
32. Yu, P.; Huang, J.; Tang, J. Observation of Coalescence Process of Silver Nanospheres during Shape Transformation to Nanoprisms. *Nanoscale Res. Lett.* **2010**, *6*, 1–7.
33. Huang, W.-L.; Chen, C.-H.; Huang, M. H. Investigation of the Growth Process of Gold Nanoplates Formed by Thermal Aqueous Solution Approach and the Synthesis

of Ultra-small Gold Nanoplates. *J. Phys. Chem. C* **2007**, *111*, 2533–2538.
34. Chung, P.-J.; Lyu, L.-M.; Huang, M. H. Seed-Mediated and Iodide-Assisted Synthesis of Gold Nanocrystals with Systematic Shape Evolution from Rhombic Dodecahedral to Octahedral Structures. *Chemistry* **2011**, *17*, 9746–9752.
35. Ghader, S.; Manteghian, M.; Kokabi, M.; Mamoory, R. S. Induction Time of Reaction Crystallization of Silver Nanoparticles. *Chem. Eng. Technol.* **2007**, *30*, 1129–1133.
36. Mullin, J. W. *Crystallization*; 4th ed.; Elsevier Butterworth-Heinemann: Oxford, U.K., 2001; Chapters 5 and 6.
37. De Yoreo, J. J.; Vekilov, P. G. Principles of Crystal Nucleation and Growth. *Rev. Mineral. Geochem.* **2003**, *54*, 57–93.
38. Shelley, E. J.; Ryan, D.; Johnson, S. R.; Couillard, M.; Fitzmaurice, D.; Nellist, P. D.; Chen, Y.; Palmer, R. E.; Preece, J. A. Dialkyl Sulfides: Novel Passivating Agents for Gold Nanoparticles. *Langmuir* **2002**, *18*, 1791–1795.
39. Schneider, C. A.; Rasband, W. S.; Eliceiri, K. W. NIH Image to ImageJ: 25 Years of Image Analysis. *Nat. Methods* **2012**, *9*, 671–675.